Bulletin of the Seismological Society of America, Vol. 99, No. 2A, pp. 794–808, April 2009, doi: 10.1785/0120080014

Regional Multistation Discriminants: Magnitude, Distance, and Amplitude Corrections, and Sources of Error

by D. N. Anderson,* W. R. Walter, D. K. Fagan, T. M. Mercier, and S. R. Taylor

Abstract Magnitude, distance, and amplitude corrections (MDAC) made to observed regional amplitudes are necessary so that what remains in the corrected amplitude is mostly information about the seismic source type. Corrected amplitudes can be used in ratios to discriminate between earthquakes and explosions. However, source effects remain that cannot easily be determined and applied as amplitude corrections, such as those due to depth, focal mechanism, local material property, and apparent stress variability. We develop a mathematical model to capture these near-source effects as random (unknown), giving an error partition of three sources: model inadequacy, station noise, and amplitude correlation. This mathematical model is the basis for a general multistation regional discriminant formulation. The standard error of the discriminant includes the variances of model inadequacy and station noise, along with amplitude correlation in its formulation. The developed methods are demonstrated for a collection of Nevada test site (NTS) events observed at regional stations (see Fig. 1). Importantly, the proposed formulation includes all corrected amplitude information through the construction of multistation discriminants. In contrast, previous studies have only computed discriminants from single stations having both *P* and *S* amplitudes. The proposed multistation approach has similarities to the well-established m_b versus M_s discriminant and represents a new paradigm for the regional discrimination problem.

Introduction

The ratio of regional *P*- and *S*-wave amplitude measurements at high frequencies can discriminate between earthquakes and explosions (e.g., Walter *et al.*, 1995; Taylor, 1996; Bottone *et al.*, 2002). An issue with using these amplitudes in a practical application is how to remove the effects due to path, site, and magnitude to emphasize the source differences. In Taylor and Hartse (1998), Taylor *et al.* (2002), and Walter and Taylor (2002), the magnitude and distance amplitude correction (MDAC) technique corrects each regional phase (e.g., P_n, P_g, S_n, and L_g) amplitude as a function of frequency in an attempt to make amplitudes independent of distance, magnitude, and station. MDAC is a simple physically based model that accounts for propagation effects such as geometrical spreading and *Q*; it also corrects observed amplitudes, assuming the scaling of an earthquake spectral model developed by Brune (1970). The idea of using an earthquake MDAC model to correct amplitudes is that spectra from an explosion will exhibit a poor fit to the model that will be apparent in an observed discriminant. Because of complex explosion source phenomenology, the combinations of regional phases that will best separate earthquake and explosion populations are not necessarily obvious. The MDAC technique allows for the formulation of any combination of regional phases in any frequency band so that a diversity of discriminants can be explored.

The MDAC model partitions regional seismic spectra into component parts. The instrument-corrected regional phase spectra can be thought of as a convolution between the source type and the path. In the frequency domain, this can be mathematically represented as

$$A(\omega, \Delta) = S(\omega)G(\Delta)P(\omega)B(\omega, \Delta), \qquad (1)$$

where *S* is the source spectrum, *G* is the geometrical spreading, *P* is the frequency-dependent site effect, and *B* is the anelastic attenuation with function arguments epicentral distance Δ and angular frequency ω. Here we have split the path effect into three components: (1) a frequency independent geometrical spreading component, (2) a range-independent and frequency-dependent site effect, and (3) an anelastic attenuation component.

*Now at Los Alamos National Laboratory, Geophysics Group, P.O. Box 1663, MS F665, Los Alamos, New Mexico 87545.

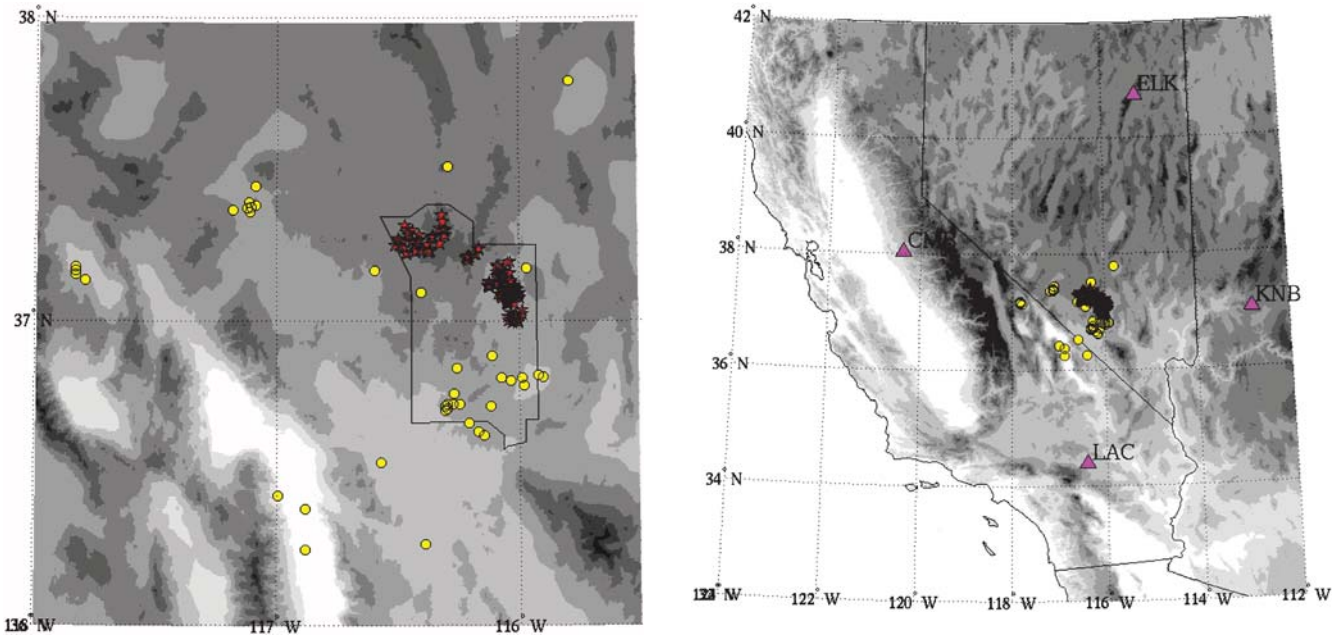

Figure 1. Maps of NTS events observed at regional distances by stations KNB, ELK, LAC, and CMB. Explosions are red and earthquakes are yellow.

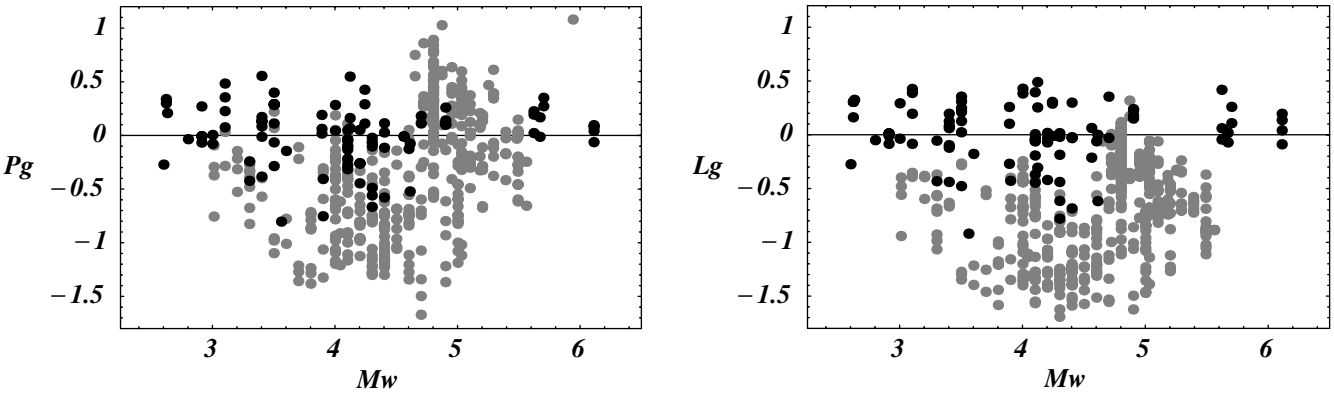

Figure 2. Scatter plot of MDAC corrected amplitudes L_g and P_g versus moment magnitude M_w for earthquakes (black dots) and explosions (gray dots). MDAC corrects earthquakes to zero mean.

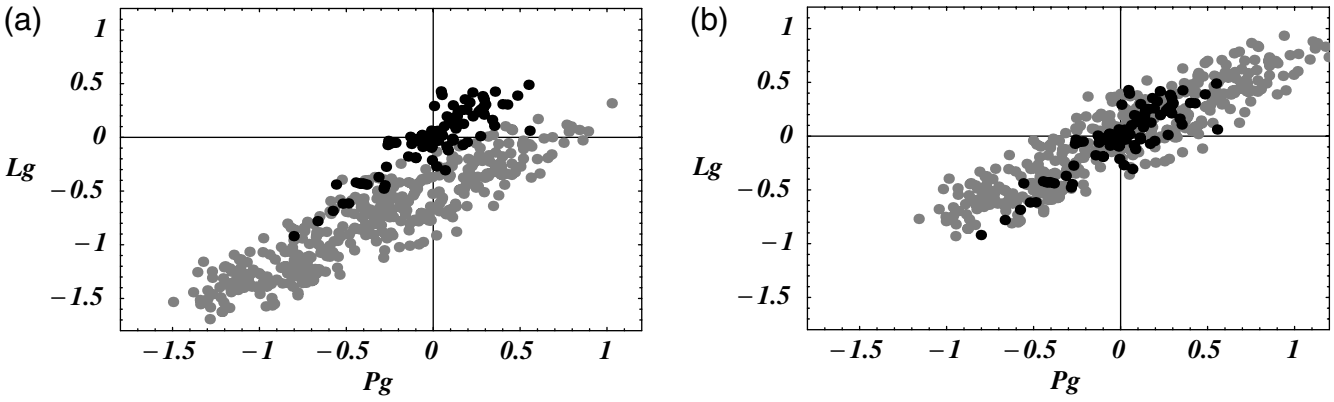

Figure 3. Scatter plot of the MDAC corrected amplitudes L_g versus P_g for earthquakes (black dots) and explosions (gray dots). Figure 3a exhibits discrimination because the earthquake and explosion populations are disjointed. With the explosions mean centered, Figure 3b shows the data that are used to calibrate the common standard error parameters (τ and σ for P_g and L_g, along with ρ) for both populations.

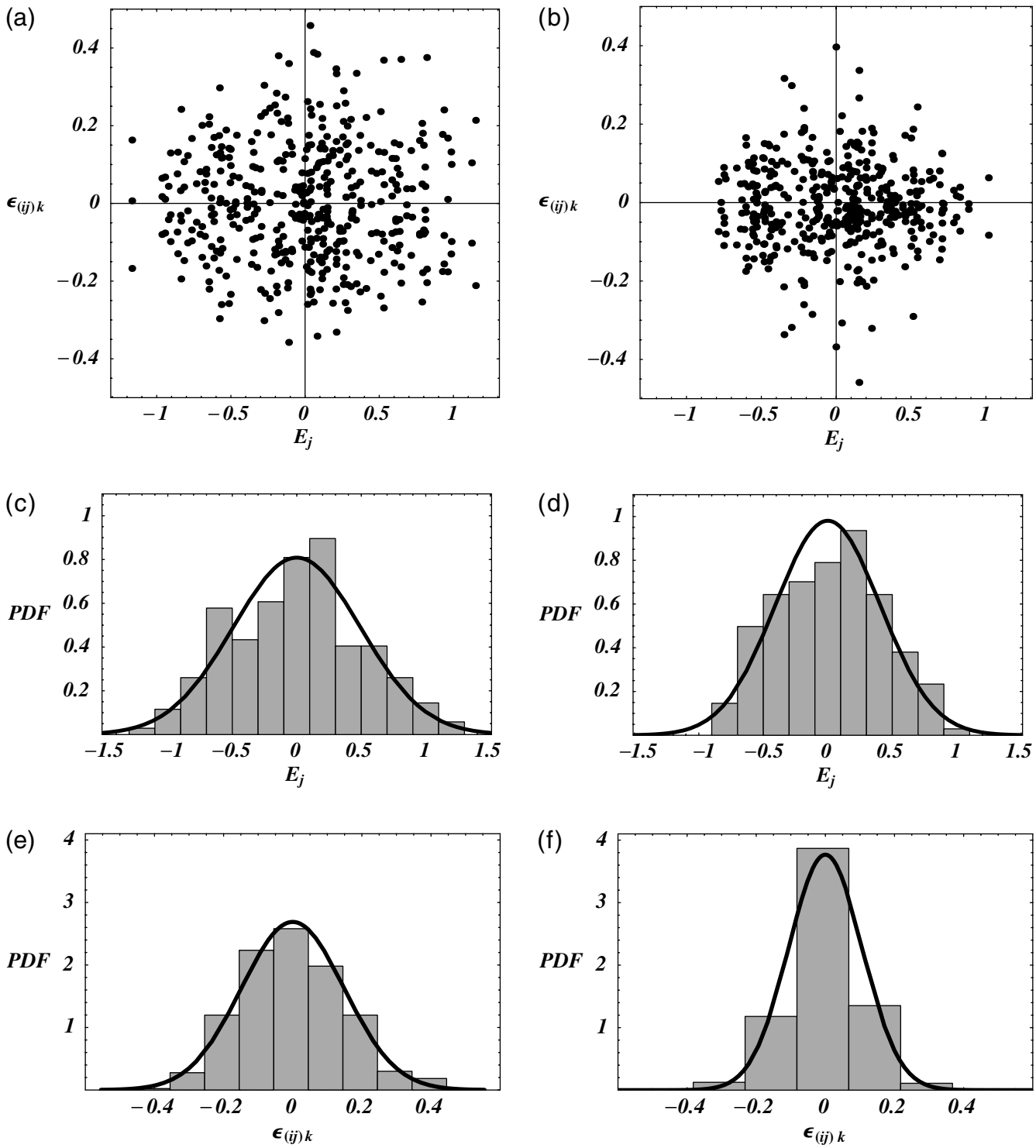

Figure 4. Validation analysis for the distributional properties of fitted E_j and $\epsilon_{(ij)k}$ for the MDAC multistation discriminant. χ^2 goodness-of-fit tests were performed with the bin size chosen to give a best fit to a normal distribution. For each test, the degrees of freedom were adjusted to account for model parameter estimation (τ, σ). All tests constrain the probability density function (PDF) mean to zero. For Figure 4c, a goodness-of-fit test returned $\chi^2 = 10.80$ with 13 degrees of freedom and a p value equal to 0.63. For Figure 4d, $\chi^2 = 10.45$ with 13 degrees of freedom and a p value equal to 0.66. For Figure 4e, $\chi^2 = 10.88$ with 9 degrees of freedom and a p value equal to 0.28. For Figure 4f, $\chi^2 = 28.73$ with 7 degrees of freedom and a p value $\approx$0.63.

The logarithm of both sides of equation (1) gives

$$\log A(\omega, \Delta) = \log S(\omega) + \log G(\Delta) + \log P(\omega) + \log B(\omega, \Delta). \quad (2)$$

To remove distance and magnitude trends in the data, we correct the observed spectrum $\log A_o(\omega, \Delta)$ so that

$$\log A_c(\omega, \Delta) = \log A_o(\omega, \Delta) - \log A(\omega, \Delta), \quad (3)$$

where $\log A_c(\omega, \Delta)$ is the corrected spectrum. Equation (3) is used to calculate corrected MDAC amplitudes, denoted as Y, that are then used to construct discriminants. Specifically, from equation (3), the corrected amplitude Y is a log-observed amplitude minus MDAC (MDAC residual).

We develop the mathematics to form a multistation discriminant constructed from the station average of the corrected amplitudes Y. The proposed discriminant is built from random effects' analysis of variance (see, e.g., Searle, 1971; Searle *et al.*, 1992) that has been applied to other path correction theories in seismology (see, e.g., Chen and Tsai, 2002; Tsai and Chen, 2003; Tsai *et al.*, 2006). We model any remaining physical structure in corrected amplitudes as a

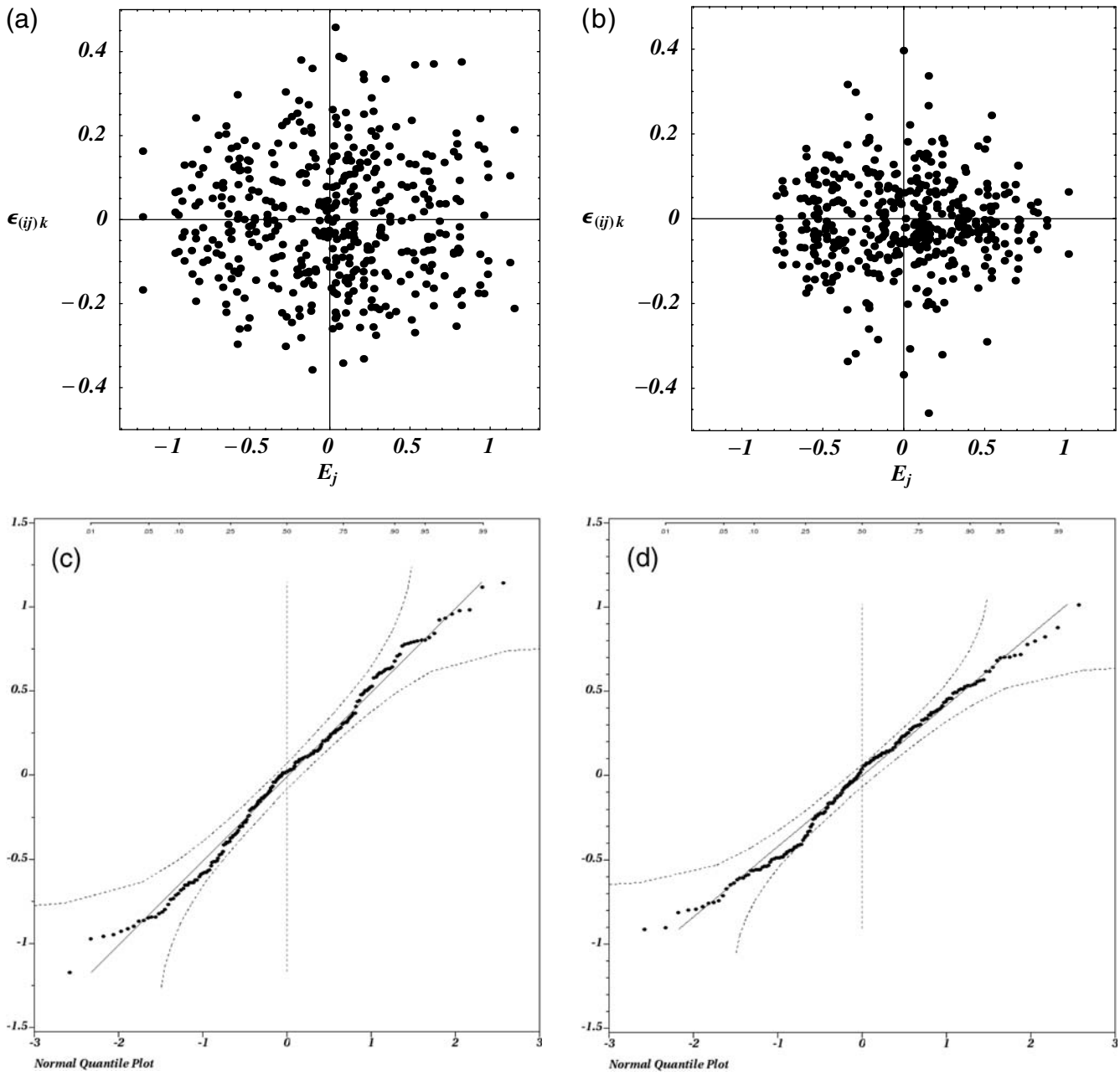

Figure 5. Normal quantile–quantile (Q–Q) plots for E_j and $\epsilon_{(ij)k}$ for the MDAC multistation discriminant. 95% confidence bounds are provided under a normal null hypothesis. Figures 5c,d are Q–Q plots of E_j for P_g and L_g, respectively. Figures 5e,f are Q–Q plots of $\epsilon_{(ij)k}$ for P_g and L_g, respectively. (*Continued*)

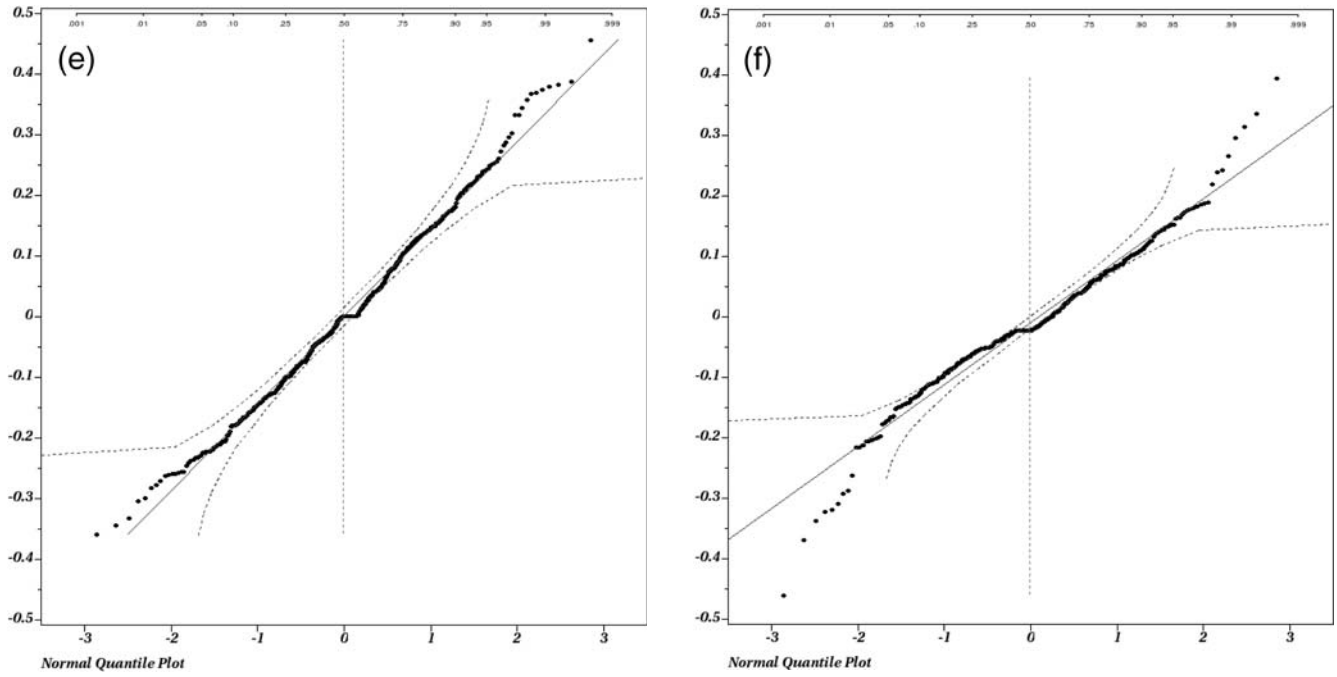

Figure 5. Continued.

source-type bias plus two random effect components—model inadequacy and station noise. This approach to discriminant formulation properly forms the standard error of the discriminant with these two variance components, along with the correlation between amplitudes forming the discriminant. Model inadequacy decreases with improvements in amplitude correction theory and improved calibration (e.g., improved MDAC parameters). Station noise is reduced through station averaging. MDAC (or any other path correction formulation) can be augmented with additional corrections; the multistation model developed here holds.

A compelling argument for using all available station information with the multistation discriminant is illustrated with a thought experiment: four stations observe signals from a clandestine nuclear explosion. Three of the four stations only observe the *P* wave (which may be the case for an explosion). The fourth station observes both *P* and *S* waves. The *P* wave at the fourth station is anomalously low, causing the discriminant to appear earthquake like, resulting in a misclassified explosion if only this station is used (e.g., it is *a priori* determined to have the best identification performance of the four). However, if all of the corrected *P*-wave amplitudes are averaged and combined with the single *S*-wave measurement, a better estimate of the actual P/S ratio is obtained and the event is correctly identified. The multistation discriminant developed here is a technically rigorous approach to resolve this apparent conflict among individual station identifications because it properly combines the corrected station amplitudes with mathematical statistics theory.

We compared individual station performance reported in Walter *et al.* (1995) to the multistation discriminant performance using a comparable MDAC model and data. Walter *et al.* (1995) report equiprobable error rates of 13.4% and 18.1% for Kanab, Utah and Mina, Nevada respectively. The multistation discriminant exhibits improved performance with an equiprobable error rate slightly less than 10%. We also validate the multistation discriminant with an analysis of model assumptions in the section entitled NTS Data

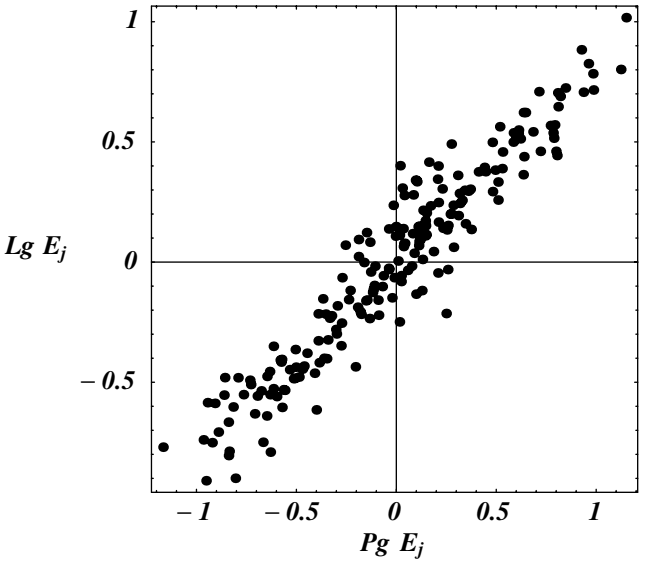

Figure 6. Bivariate plot of fitted E_j values for P_g and L_g. The calculated correlation $\rho = 0.95$.

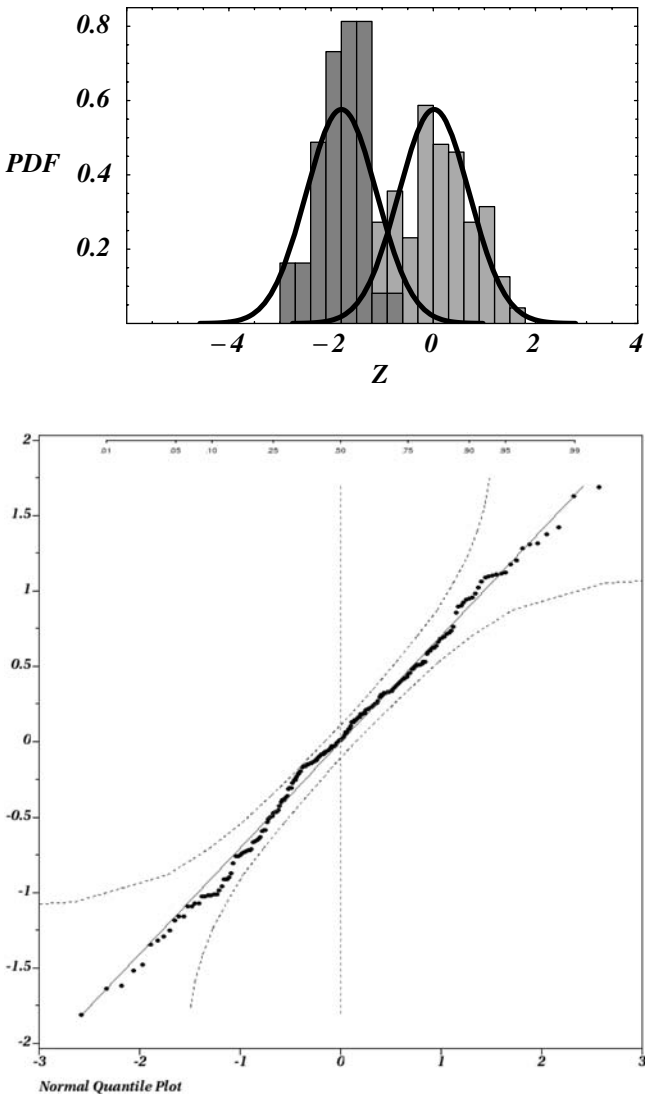

Figure 7. Fitted PDF models of the multistation MDAC discriminant $Z_{\bar{P}_g - \bar{L}_g}$ for earthquakes (black histogram) and explosions (gray histogram). The explosion population mean is ≈ 0 and the earthquake population mean is -1.80. The pooled standard deviation for the populations is 0.69. The Q–Q plot is of the pooled earthquake and explosion data (centered to their respective source-type means), and it confirms that the earthquake and explosion data are reasonably modeled as normal with equal variance.

Analysis with the MDAC Multistation Discriminant. The section entitled NTS Data Analysis with a Regression Correction Multistation Discriminant demonstrates that the multistation discriminant is also applicable to other amplitude correction methods used in discrimination analysis, specifically regression corrections on station discriminants. In the section titled Cross-Validation Analysis: MDAC Multistation Discriminant versus Best Single Station, we present the results of a cross-validation study that compares the multistation discriminant performance to that of a best single-station identification method. The cross-validation analysis demonstrates a significantly improved performance with the multistation discriminant. We note that the same MDAC correction is used throughout this article.

Table 1

Estimates of Model Error (τ^2) and Station Error (σ^2) for MDAC Corrected P_g and L_g Amplitudes

Phase	Model Error	Station Error
P_g	0.23	0.04
L_g	0.16	0.02

From Figure 6, the estimated correlation between P_g and L_g is $\rho = 0.95$.

The multistation regional discriminant is analogous to the formulation of the m_b versus M_s discriminant used for decades in seismic event identification (see Blandford, 1982). To see this, we note that the calculation of a corrected amplitude (equation 3) is very similar to the calculation of a station m_b or M_s. In the m_b versus M_s discriminant, station-averaged magnitudes are used with potentially differing sets of stations in the calculation of each. Similarly, the multistation regional discriminant proposed here is also constructed from station-averaged corrected amplitudes with potentially differing stations used in each.

The MDAC Discriminant: Model Inadequacy and Station Noise

Until now, no attempt has been made to obtain a realistic estimate of the error budget associated with corrected amplitudes. Established signal processing research treats amplitudes as lognormally distributed; therefore, in log space, properly formed differences are normal (Gaussian) discriminants. The conceptual representation of the proposed model is

$$\begin{aligned} Y &= \log(\text{corrected amplitude}) \\ &= \text{bias(source type)} + \text{event} + \text{noise}, \end{aligned} \tag{4}$$

where bias (source type) is a source-type constant, event is a zero mean random effect that varies from event to event and represents model inadequacy from effects such as depth, focal mechanism, local material property, and apparent stress variability, and noise represents measurement and ambient noise, also with zero mean. The MDAC approach results in a bias term for earthquakes that is near zero, whereas for explosions the bias is nonzero, indicating discrimination potential. Equation (4) implies that the expected value of Y is

$$\mathcal{E}\{Y\} = \text{bias(source type)}. \tag{5}$$

Table 2

Source-Type Bias (Average) for MDAC Corrected P_g and L_g Amplitudes

Bias	EX($i = 1$)	EQ($i = 0$)
μ_{P_g}	−0.34	0
μ_{L_g}	−0.76	0

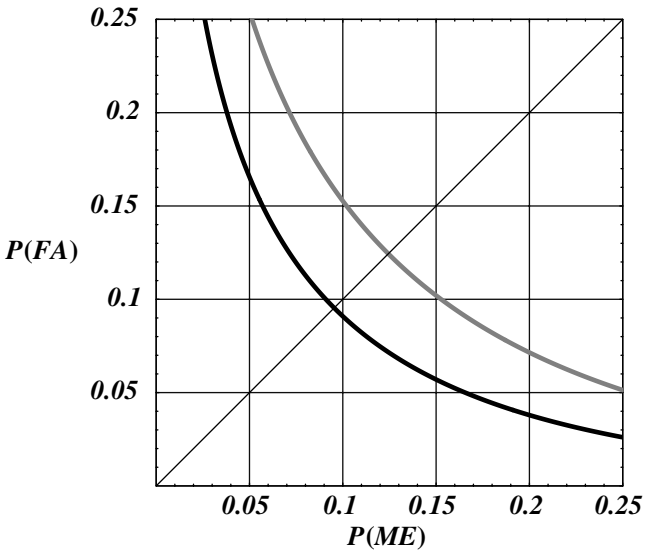

Figure 8. Receiver operation curves (ROC) for multistation MDAC (black line) and multistation regression correction (gray line) discrimination. The equiprobable error, identified by the 45° line, is ≈10% for MDAC discrimination and ≈12.5% for regression discrimination. FA denotes false alarm and ME denotes missed explosion.

In the development, it is assumed that data quality metrics have been applied, thereby giving high levels of confidence in the quality of the observed amplitudes.

For the mathematical statistics formulation of equation (4), define the random variable Y_{ijk} to be the corrected amplitude for source type $i = 0, 1$ (earthquake, explosion), event j, and station k (observed data are denoted y_{ijk}). The linear model representation of equation (4) is then

$$Y_{ijk} = \mu_i + E_j + \epsilon_{(ij)k}, \qquad j = 1, 2, \ldots m_i, \quad k = 1, 2, \ldots n_{ij}. \tag{6}$$

Analogous to equation (4), equation (6) reads Y_{ijk} equals a constant source-type bias μ_i plus a random event adjustment

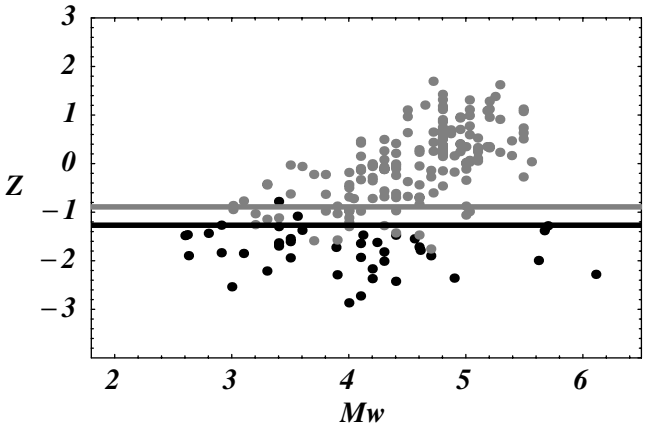

Figure 9. Scatter plot of observed MDAC multistation discriminants versus M_w. Earthquakes are black dots and explosions are gray dots. The decision thresholds are $\ell_{\text{model}} = -0.89$ (gray dots) and $\ell_{\text{empirical}} = -1.27$ (black dots). Performance counts are reported in Tables 3 and 4.

Table 3

Identification Performance of the MDAC Multistation Discriminant in Equation (14) with the Model-Based Decision Line $\ell_{\text{model}} = -0.89$

	$\widehat{\text{EX}}$	$\widehat{\text{EQ}}$
EX	137	22
EQ	1	40

Rows are the true source type and columns are the identified source.

Table 4

Identification Performance of the MDAC Multistation Discriminant in Equation (14) with the Empirical-Based Decision Line $\ell_{\text{empirical}} = -1.27$

	$\widehat{\text{EX}}$	$\widehat{\text{EQ}}$
EX	152	7
EQ	2	39

Rows are the true source type and columns are the identified source.

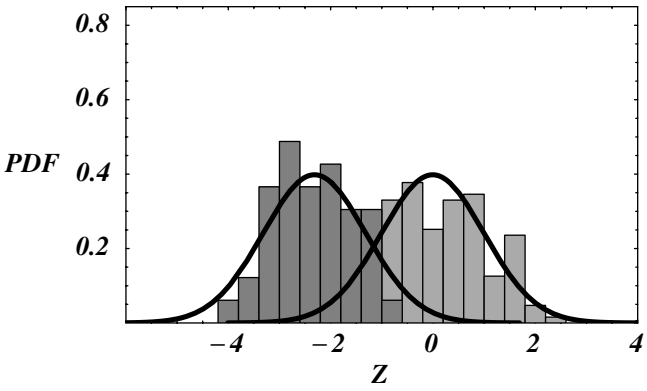

Figure 10. Fitted models of the multistation regression correction discriminant $Z_{\bar{X}}$ for earthquakes (black histogram) and explosions (gray histogram). The explosion population mean is ≈0 and the earthquake population mean is −2.32. The pooled standard deviation for the populations is 1.00.

Table 5

Estimates of Model Error (τ^2) and Station Error (σ^2) for the Regression Corrected Station Discriminants $X = P_g - L_g$

Phase	Model Error	Station Error
$X = P_g - L_g$	0.009	0.034

Table 6

Source-Type Bias (Average) for the Regression Corrected Station Discriminant $X = P_g - L_g$

Bias	EX ($i = 1$)	EQ ($i = 0$)
$X = P_g - L_g$	0.368	0

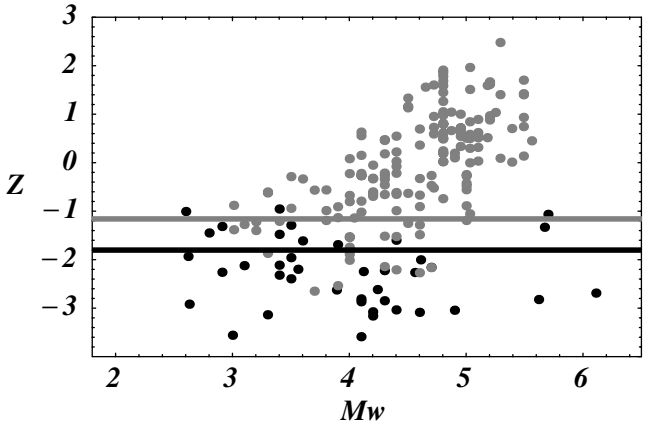

Figure 11. Scatter plot of observed regression corrected multistation discriminants versus M_w. Earthquakes are black dots and explosions are gray dots. The decision thresholds are $\ell_{\text{model}} = -1.16$ (gray line) and $\ell_{\text{empirical}} = -1.80$ (black line). Performance counts are reported in Tables 7 and 8.

E_j (model inadequacy due to local source effects) plus a station noise adjustment $\epsilon_{(ij)k}$. The subscript notation $(ij)k$ for ϵ specifies that station noise is different for each source type and event combination. Equation (6) is a standard mixed effects (random and fixed) linear model (see Searle, 1971; Searle *et al.*, 1992).

The E_j are modeled as independent normal random variables with zero mean and variance τ^2. The $\epsilon_{(ij)k}$ are independent normal random variables with zero mean and variance σ^2. E_j and $\epsilon_{(ij)k}$ are independent across all subscripts. This assumption is consistent with effects local to the source being uncorrelated with station noise. As an example, for two stations and three events the statistical properties of E_j and $\epsilon_{(ij)k}$ are succinctly written as

$$\begin{pmatrix} E_1 \\ \epsilon_{(i1)1} \\ \epsilon_{(i1)2} \\ E_2 \\ \epsilon_{(i2)1} \\ \epsilon_{(i2)2} \\ E_3 \\ \epsilon_{(i3)1} \\ \epsilon_{(i3)2} \end{pmatrix} \text{ is normal}(\mathbf{0}, \boldsymbol{\Sigma}),$$

$$\boldsymbol{\Sigma} = \begin{pmatrix} \tau^2 & 0 & 0 & 0 & 0 & 0 & 0 & 0 & 0 \\ 0 & \sigma^2 & 0 & 0 & 0 & 0 & 0 & 0 & 0 \\ 0 & 0 & \sigma^2 & 0 & 0 & 0 & 0 & 0 & 0 \\ 0 & 0 & 0 & \tau^2 & 0 & 0 & 0 & 0 & 0 \\ 0 & 0 & 0 & 0 & \sigma^2 & 0 & 0 & 0 & 0 \\ 0 & 0 & 0 & 0 & 0 & \sigma^2 & 0 & 0 & 0 \\ 0 & 0 & 0 & 0 & 0 & 0 & \tau^2 & 0 & 0 \\ 0 & 0 & 0 & 0 & 0 & 0 & 0 & \sigma^2 & 0 \\ 0 & 0 & 0 & 0 & 0 & 0 & 0 & 0 & \sigma^2 \end{pmatrix}, \tag{7}$$

where $\mathbf{0}$ denotes a zero mean vector and $\boldsymbol{\Sigma}$ is the covariance matrix of the model error components.

Define the indicator matrix

$$\mathbf{W} = \begin{pmatrix} 1 & 1 & 0 & 0 & 0 & 0 & 0 & 0 & 0 \\ 1 & 0 & 1 & 0 & 0 & 0 & 0 & 0 & 0 \\ 0 & 0 & 0 & 1 & 1 & 0 & 0 & 0 & 0 \\ 0 & 0 & 0 & 1 & 0 & 1 & 0 & 0 & 0 \\ 0 & 0 & 0 & 0 & 0 & 0 & 1 & 1 & 0 \\ 0 & 0 & 0 & 0 & 0 & 0 & 1 & 0 & 1 \end{pmatrix} \tag{8}$$

to select appropriate vector/matrix elements for the matrix representation of equation (6). Then

$$\begin{pmatrix} Y_{i11} \\ Y_{i12} \\ Y_{i21} \\ Y_{i22} \\ Y_{i31} \\ Y_{i32} \end{pmatrix} = \begin{pmatrix} \mu_i \\ \mu_i \\ \mu_i \\ \mu_i \\ \mu_i \\ \mu_i \end{pmatrix} + \begin{pmatrix} 1 & 1 & 0 & 0 & 0 & 0 & 0 & 0 & 0 \\ 1 & 0 & 1 & 0 & 0 & 0 & 0 & 0 & 0 \\ 0 & 0 & 0 & 1 & 1 & 0 & 0 & 0 & 0 \\ 0 & 0 & 0 & 1 & 0 & 1 & 0 & 0 & 0 \\ 0 & 0 & 0 & 0 & 0 & 0 & 1 & 1 & 0 \\ 0 & 0 & 0 & 0 & 0 & 0 & 1 & 0 & 1 \end{pmatrix} \begin{pmatrix} E_1 \\ \epsilon_{(i1)1} \\ \epsilon_{(i1)2} \\ E_2 \\ \epsilon_{(i2)1} \\ \epsilon_{(i2)2} \\ E_3 \\ \epsilon_{(i3)1} \\ \epsilon_{(i3)2} \end{pmatrix} \tag{9}$$

is normal $(\boldsymbol{\Theta}, \boldsymbol{\Omega})$, where the mean vector $\boldsymbol{\Theta}$ and covariance matrix $\boldsymbol{\Omega}$ are

Table 7

Identification Performance of the Regression Correction Multistation Discriminant in Equation (17) with the Model-Based Decision Line $\ell_{\text{model}} = -1.16$

	$\widehat{\text{EX}}$	$\widehat{\text{EQ}}$
EX	135	24
EQ	3	38

Rows are the true source type and columns are the identified source.

Table 8

Identification Performance of the Regression Corrected Multistation Discriminant in Equation (17) with the Empirical-Based decision Line $\ell_{\text{empirical}} = -1.80$

	$\widehat{\text{EX}}$	$\widehat{\text{EQ}}$
EX	150	9
EQ	11	30

Rows are the true source type and columns are the identified source.

$$\boldsymbol{\Theta} = \begin{pmatrix} \mu_i \\ \mu_i \\ \mu_i \\ \mu_i \\ \mu_i \\ \mu_i \end{pmatrix} \quad \text{and} \quad \boldsymbol{\Omega} = \mathbf{W}\boldsymbol{\Sigma}\mathbf{W}' = \begin{pmatrix} \tau^2+\sigma^2 & \tau^2 & 0 & 0 & 0 & 0 \\ \tau^2 & \tau^2+\sigma^2 & 0 & 0 & 0 & 0 \\ 0 & 0 & \tau^2+\sigma^2 & \tau^2 & 0 & 0 \\ 0 & 0 & \tau^2 & \tau^2+\sigma^2 & 0 & 0 \\ 0 & 0 & 0 & 0 & \tau^2+\sigma^2 & \tau^2 \\ 0 & 0 & 0 & 0 & \tau^2 & \tau^2+\sigma^2 \end{pmatrix}. \tag{10}$$

This two station and three event example is easily generalized across source types i, events $j = 1, 2, \ldots, m_i$, and stations $k = 1, 2, \ldots, n_{ij}$.

Two corrected amplitudes Y_{ijk} and Y^*_{ijk} are used for regional discriminants, and they can be correlated. For example, Y_{ijk} could be a corrected P-wave amplitude and Y^*_{ijk} a corrected S-wave amplitude. From equation (6), the random mechanism causing this correlation is modeled with the E_j term because it equally perturbs the signal at all stations observing an event, along with the measured amplitudes. Conceptually extending the example given in equation (7) to two amplitudes gives a block diagonal covariance matrix with the $(1, 1)$ block for Y_{ijk} as previously described and the $(2, 2)$ block for Y^*_{ijk} analogous to the previously described terms. Introducing a correlation ρ (covariance) in the off-diagonal blocks between the E terms for Y_{ijk} and Y^*_{ijk} provides the statistical model to calculate the standard error of the multistation discriminant given in the Discriminant Formulation section. Calibration data y_{ijk} and y^*_{ijk} are from events observed by stations for both source types. For the analysis examples in the sections entitled NTS Data Analysis with the MDAC Multistation Discriminant and NTS Data Analysis with a Regression Correction Multistation Discriminant, along with the cross-validation study of the Cross-Validation Analysis: MDAC Multistation Discriminant versus Best Single Station, established methods are used to estimate the variance components (τ, σ) and amplitude correlation (ρ) (see, e.g., Searle, 1971; Searle *et al.*, 1992).

Statistical Properties of a Station-Averaged MDAC Residual

For source type i and event j, denote the $1 \times n_{ij}$ vector of corrected amplitudes as $\mathbf{Y}'_{ij} = (Y_{ij1}, Y_{ij2}, \ldots, Y_{ijn_{ij}})$. Then, generalizing to n_{ij} stations, $\mathbf{Y}_{ij}$ is multivariate normal with $1 \times n_{ij}$ mean vector $\boldsymbol{\Theta}'_{ij} = (\mu_i, \mu_i, \ldots, \mu_i)$ and $n_{ij} \times n_{ij}$ covariance matrix

$$\boldsymbol{\Omega}_{ij} = \begin{pmatrix} \tau^2+\sigma^2 & \tau^2 & \tau^2 & \cdots & \tau^2 \\ \tau^2 & \tau^2+\sigma^2 & \tau^2 & & \tau^2 \\ \tau^2 & \tau^2 & \ddots & & \vdots \\ \vdots & & & \tau^2+\sigma^2 & \tau^2 \\ \tau^2 & \cdots & \tau^2 & \tau^2 & \tau^2+\sigma^2 \end{pmatrix}. \tag{11}$$

The station-averaged corrected amplitude $\bar{Y}_{ij} = \underline{1}'\underline{\mathbf{Y}}_{ij}/n_{ij}$ is normal with mean μ_i and standard error $\tau^2 + \sigma^2/n_{ij}$. Note that forming regional discriminants from station-averaged corrected amplitudes exactly parallels the methodology of the m_b versus M_s discriminant where both are station-averaged magnitudes.

Omitting the term E_j in equation (6) implies that the corrected amplitude at a station is μ_i plus station noise. As demonstrated with the following argument, this model formulation is fundamentally inconsistent with the realities of seismic observation. The standard error of $\bar{Y}_{ij}$ with E_j removed from equation (6) is σ^2/n_{ij} ($\tau^2 = 0$) and decreases as the number of stations n_{ij} observing an event increases. This implies that if enough stations observe an event, this standard error effectively goes to zero and the average corrected amplitude quickly converges to μ_i, implying near-perfect discrimination capability. By not including the term E_j, effects such as depth, focal mechanism, local material property, and apparent stress variability are not accounted for in the theoretical model of an amplitude; clearly these effects cannot be removed by station averaging. The model given by equation (6) captures these local source effects by admitting that they cannot be mathematically (theoretically) represented. Treating local source effects as a random effect (E_j) compensates for them as a component in the standard error of a discriminant. Also, the lower bound of equation (6) is nonzero and therefore consistent with realistic seismic monitoring.

Another important property of this model is that a corrected amplitude for a single event is correlated across stations. The correlation $[\tau^2/(\tau^2 + \sigma^2)]$ implies that large adjustment E_j increases correlation between stations because this random adjustment is applied to all stations observing an event, that is, the stations stochastically move together. Small adjustment E_j implies the correction model is good and is conceptually equivalent to stations with incoherent noise. Small adjustment E_j also implies that τ^2 is small and the standard error of $\bar{Y}_{ij}$ is reduced further through station averaging.

Discriminant Formulation

A discriminant is constructed from two different station-averaged amplitudes $\bar{Y}_{ij}$ and $\bar{Y}^*_{ij}$ (with different bias constants μ_i and μ^*_i). For specific regional phases, the discriminant equation can be represented with meaningful subscripts. For example, for a given event with source type i, the station-averaged corrected amplitude $\bar{P}_g$ is normal with mean

μ_{i,P_g} and standard error $\tau^2_{P_g} + \sigma^2_{P_g}/n_{P_g}$, and $\bar{L}_g$ is normal with mean μ_{i,L_g} and standard error $\tau^2_{L_g} + \sigma^2_{L_g}/n_{L_g}$. Note that if only stations observing a discriminant are used, then $n_{P_g} = n_{L_g}$; however, this constraint on discriminant construction is not necessary—using all available data to construct a discriminant is theoretically sound with good instrument and amplitude corrections. With the inclusion of correlation ρ between amplitudes, the standard error of the P_g versus L_g discriminant is

$$SE_{\bar{P}_g - \bar{L}_g} = \sqrt{\tau^2_{P_g} + \frac{\sigma^2_{P_g}}{n_{P_g}} + \tau^2_{L_g} + \frac{\sigma^2_{L_g}}{n_{L_g}} - 2\rho\tau_{P_g}\tau_{L_g}} \quad (12)$$

for both earthquakes and explosions. Equality of the standard error for both source types is an important model property because unlike discrimination analysis with unequal source variability, it ensures that an earthquake with an unusually strong earthquake-identifying discriminant value will not be identified as an explosion. This can occur with discrimination methods that model source-type variance as unequal (see McLachlan, 1992)—explosion calibration data can exhibit variability that is significantly larger than earthquake calibration data.

Current physical correction theory is unable to adjust amplitudes for all local effects. The NTS Data Analysis with the MDAC Multistation Discriminant section demonstrates removal of M_w with MDAC amplitudes; however, a clear correlation between observed MDAC amplitudes is shown, which agrees well with the multistation model equation (6). Local physical corrections are modeled as random and, as previously discussed, these local effects move out to all stations (and therefore amplitudes), hence the correlation. When physical corrections for local effects are possible, the model inadequacy terms E_j will be small, giving small values of τ, and the covariance between amplitudes will be small. In the limit, this conceptually gives discriminant amplitude scatter plots for explosions and earthquakes (populations) that are small shotgun patterns of data; the discrimination problem becomes one of physical correction and station noise.

Centering the multistation discriminant relative to some constant and adjusting for uncertainty gives a standardized discriminant. For example, centering relative to the explosion population mean $\mu_{1,P_g} - \mu_{1,L_g}$ forms the standardized discriminant

$$Z_{\bar{P}_g - \bar{L}_g} = \frac{(\bar{P}_g - \mu_{1,P_g}) - (\bar{L}_g - \mu_{1,L_g})}{\sqrt{\tau^2_{P_g} + \sigma^2_{P_g}/n_{P_g} + \tau^2_{L_g} + \sigma^2_{L_g}/n_{L_g} - 2\rho\tau_{P_g}\tau_{L_g}}}, \quad (13)$$

which is centered at zero for explosions and has a nonzero center for earthquakes. Equation (6) mathematically formalizes the MDAC approach to regional discrimination and fundamentally bases source-type identification performance on differences between the bias constants μ_i and μ_i^*. The advantage to centering relative to explosions is consistency with the monitoring position to assume all events are explosions and then prove otherwise with seismic signatures.

Equation (6) also implies that $Z_{\bar{P}_g - \bar{L}_g}$ has the same variance for both populations. As previously noted, imposing equal population variances is driven by physical basis considerations so that an explosion with an unusually strong explosion-identifying discriminant value will not be identified as an earthquake, as could be the case with quadratic discrimination rules.

From equation (13), values of $Z_{\bar{P}_g - \bar{L}_g}$ less than a decision threshold predict an earthquake as the source-type identification (otherwise explosion). The section entitled NTS Data Analysis with the MDAC Multistation Discriminant illustrates performance with two decision thresholds: a model-based threshold that gives equal missed-explosion and false-alarm error rates and an empirical decision threshold. The model-based threshold is the average of the means of $Z_{\bar{P}_g - \bar{L}_g}$ for explosions and earthquakes. The empirical-based threshold is simply the average of the largest earthquake Z and the smallest explosion Z. The empirical-based decision threshold is derived from the tail behavior of the observed data and can be strongly influenced by the empirical distribution of the calibration data. The model-based threshold is derived from the fit of model parameters to calibration data. In the NTS Data Analysis with the MDAC Multistation Discriminant and NTS Data Analysis with a Re-

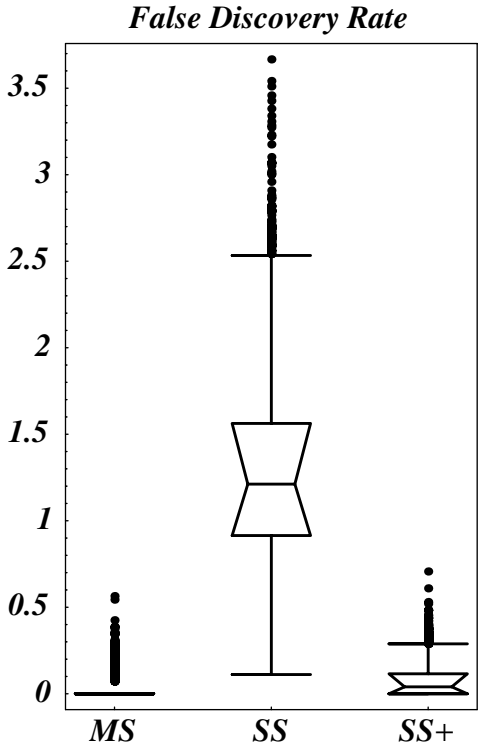

Figure 12. Box plots of 5000 cross-validated values of the FDR for the multistation (MS) discriminant, along with the single-station (SS) and single-station plus (SS+) approaches to regional discrimination.

gression Correction Multistation Discriminant sections, we provide both to illustrate the difference.

NTS Data Analysis with the MDAC Multistation Discriminant

Amplitude corrections for discrimination remove the effects of magnitude, source scaling, and distance so that what fundamentally remains in the corrected amplitude is information about source type. Figure 2 demonstrates the removal of the effect of moment magnitude M_w from the P_g and L_g amplitudes with MDAC. Note that the earthquakes are mean centered to zero. With amplitude corrections, there is often correlation between the amplitudes used to form a discriminant. Figure 3a shows MDAC corrected P_g and L_g data for earthquakes and explosions. The earthquake data exhibit more L_g energy consistent with the physical basis of the P_g versus L_g discriminant. The model equation (6) assumes that the earthquake and explosion populations have equal covariance matrices for all events; under this assumption, the calibration data are given in Figure 3b. These data are used to compute the model parameters for equation (6).

For both earthquakes and explosions, E_j and $\epsilon_{(ij)k}$ are modeled as zero mean with variances τ^2 and σ^2, respectively. The assumption that the model terms E_j and $\epsilon_{(ij)k}$ are uncorrelated is conceptually valid because E_j represents source model inadequacy; stations (and therefore station noise) are at least 100 km from the source. Fitting equation (6) to the NTS data in Figure 3b provides calculated values of E_j and $\epsilon_{(ij)k}$. The distributional properties of these calculated model terms is provided in Figure 4. The χ^2 goodness-of-fit tests confirm that E_j and $\epsilon_{(ij)k}$ are reasonably modeled as normal random variables. The $\epsilon_{(ij)k}$ for L_g (Fig. 4f) have individual χ^2 values for the tail cells that are unusually large; with these removed, the goodness-of-fit test returned $\chi^2 = 8.05$ with three degrees of freedom and a p value ≈ 0.04. This test indicates that the $\epsilon_{(ij)k}$ for L_g exhibits some kurtosis; however, the residuals are reasonably bell shaped and are consistent with the normal assumption. Figure 5 gives quantile–quantile (Q–Q) plots that further confirm that E_j and $\epsilon_{(ij)k}$ are reasonably modeled as normal random variables. The 95% confidence bounds on the Q–Q plots are simulated (Lilliefors, 1967). Figure 6 empirically shows the correlation between model inadequacy E_j for the two amplitudes. These data provide the value for the model parameter ρ.

The fitted population models for $Z_{\bar{P}_g - \bar{L}_g}$ with equal (pooled) variance of 0.48 are presented in Figure 7. A goodness-of-fit test applied to the explosion population returned $\chi^2 = 16.28$ with 15 degrees of freedom and a p value of 0.36. A goodness-of-fit test applied to the earthquake population returned $\chi^2 = 13.31$ with 15 degrees of freedom and a p value of 0.58. These two tests indicate that the equal population variance and normal assumptions for equation (6) are reasonable.

Estimated model parameters are provided in Tables 1 and 2. Using the fitted models, the decision threshold is $\ell_{\text{model}} = -0.89$. From the receiver operation characteristic (ROC) curve in Figure 8, the equiprobable error is $\approx$10%. The empirical decision threshold is $\ell_{\text{empirical}} = -1.27$. Figure 9 is a plot of the observed discriminants $Z_{\bar{P}_g - \bar{L}_g}$ versus M_w, with $\ell_{\text{empirical}}$ and ℓ_{model}. The empirical-based decision threshold is derived from the tail behavior of the observed data and can be strongly influenced by the empirical distribution of the calibration data. The model-based threshold is derived from the fit of model parameters to calibration data. The performance from Figure 9 is provided in Tables 3 and 4. In this analysis, performance is reported as apparent (see McLachlan, 1992), that is, all data were used to calculate model parameters and then discrimination analysis, using all data, was performed with these same parameters. In the section titled Cross-Validation Analysis: MDAC Multistation Discriminant versus Best Single Station, the MDAC multistation discriminant is shown to have better performance than that of a best single-station approach with a comprehensive cross-validation study.

Figure 9 suggests the possibility of a correlation between Z and M_w for explosions. There is well-documented dependence of the P_g versus L_g discriminant on material properties at NTS (see Fig. 6 in Walter *et al.*, 1995). Explosions detonated below the water table in high-strength media have larger P_g versus L_g values than those detonated above the water table in lower strength media (see Fig. 10 in Walter

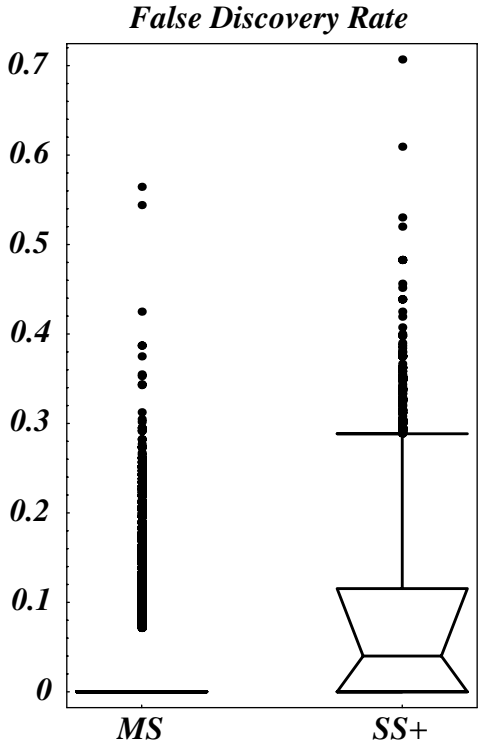

Figure 13. Box plots of 5000 cross-validated values of the FDR for the multistation (MS) discriminant and the single-station plus (SS+) approaches to regional discrimination.

et al., 1995). Containment practices at NTS dictate that larger explosions are conducted at greater depths. Therefore, M_w is actually acting as a surrogate for a rapid change in material properties occurring near the water table encountered by larger and more deeply buried explosions. The apparent differences in compression to shear energy scaling for explosions and earthquakes are also observed in published (and widely used) developments of the m_b versus M_s discriminant (see Stevens and Day, 1985; Taylor, 1996; Bonner *et al.*, 2006). The apparent correlation between Z and M_w is fundamentally due to sampling bias for the explosion population—there are no large shallow explosions and no small deep explosions in this data set. Were the explosion population to have these events, the apparent correlation would not be present. Even with this sampling bias, the assumptions for equation (6) are valid as demonstrated in the previous paragraphs—both the earthquake and explosion populations can be reasonably modeled as bivariate normal with normal marginal distributions.

NTS Data Analysis with a Regression Correction Multistation Discriminant

Prior to the MDAC formulation, discriminants were formed by first calculating a spectral ratio in a common frequency band at each station observing the event (see Blandford, 1982). These station-centric discriminants are known to be robust to instrument response calibration, and this calculation also removes the effect of magnitude. In the literature, station discriminants are then corrected for distance with a regression model built from earthquake calibration data (see Hartse *et al.*, 1997; Bottone *et al.*, 2002). Analogous to the development in the section titled The MDAC Discriminant: Model Inadequacy and Station Noise, define the random variable X_{ijk} to be the regression corrected station discriminant for source type $i = 0, 1$ (earthquake, explosion), event j, and station k (observed station discriminants are denoted x_{ijk}). Then

$$X_{ijk} = \mu_i + E_j + \epsilon_{(ij)k}, \qquad j = 1, 2, \ldots m_i, \quad k = 1, 2, \ldots n_{ij}. \tag{14}$$

For an event with n_X station discriminants, the event discriminant is the average of station discriminants $\bar{X}_{ij}$ and the standard error is

$$SE_{\bar{X}} = \sqrt{\tau^2 + \frac{\sigma^2}{n_X}} \tag{15}$$

for both earthquakes and explosions. Note that in the multistation discriminant, n_{P_g} and n_{L_g} amplitudes are averaged. Centering relative to the explosion population mean $\mu_{1,X}$ forms the standardized discriminant

$$Z_{\bar{X}} = \frac{\bar{X} - \mu_{1,X}}{\sqrt{\tau^2 + \frac{\sigma^2}{n_X}}}, \tag{16}$$

which is centered at zero for explosions and has a nonzero center for earthquakes.

In the context of this article, we calculate the difference of the observed station amplitudes P_g and L_g. We then distance correct these station discriminants with Δ and $\log \Delta$ as regressor variables (see Hartse *et al.*, 1997; Bottone *et al.*, 2002). Applying this regression model to all events gives distance corrected station discriminants X_{ijk}—the residuals. The fitted population models for $Z_{\bar{X}}$ are presented in Figure 10. Estimated model parameters are provided in Tables 5 and 6. Using these fitted models, the decision threshold is $\ell_{\text{model}} = -1.16$. From the receiver operation characteristic (ROC) curve in Figure 8, the equiprobable error is $\approx 12.5\%$. The empirical decision threshold is $\ell_{\text{empirical}} = -1.80$. Figure 11 is a plot of the observed discriminants $Z_{\bar{P}_g - \bar{L}_g}$ versus M_w, with $\ell_{\text{empirical}}$ and ℓ_{model}. The performance from Figure 11 is provided in Tables 7 and 8. As with the MDAC analysis in the NTS Data Analysis with the MDAC Multistation Discriminant section, performance is apparent. Note that the sampling characteristics of the explosion population discussed in the section are also prevalent with regression corrected station discriminants. The MDAC approach has better

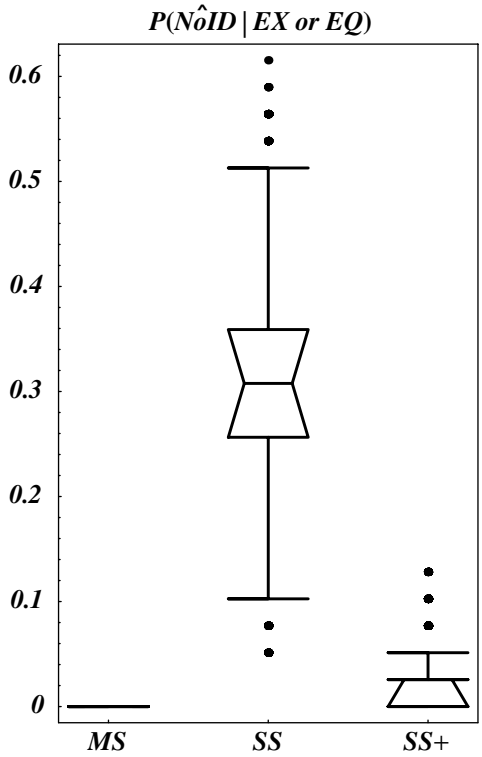

Figure 14. Operational burden for the multistation (MS) discriminant, along with the single-station (SS) and single-station plus (SS+) approaches to regional discrimination. Box plots are from 5000 cross-validated values of the $P(\widehat{\text{NoID}}|\text{EX}) + P(\widehat{\text{NoID}}|\text{EQ})$ component of operational burden.

performance than the regression correction approach presented in this section—7/159 missed explosions versus 9/159 with an empirical decision line and 2/41 false alarms versus 11/41 with an empirical decision line. Missed explosions are a serious error in the context of the treaty verification standard to miss no explosions, and from this perspective, the MDAC multistation discriminant is a significant improvement to regional seismic event identification.

Cross-Validation Analysis: MDAC Multistation Discriminant versus Best Single Station

We performed a cross-validation study to demonstrate that the multistation discriminant results in improved performance over a best single-station approach. A third approach was also investigated and compared: for events not observed by the best single station, it used information from the other stations to make an event identification. We have called this approach single station plus.

The figure of merit used in our analysis is the false discovery rate (FDR), a metric that balances operational burden (numerator) with the probability of correctly identifying an explosion (denominator). Operational burden has two components: the probability of identifying an earthquake as an explosion and the probability of being unable to determine source type because of missing measurements. Specifically,

$$\mathrm{FDR} = \frac{P(\widehat{\mathrm{EX}}|\mathrm{EQ}) + P(\widehat{\mathrm{NoID}}|\mathrm{EX}) + P(\widehat{\mathrm{NoID}}|\mathrm{EQ})}{P(\widehat{\mathrm{EX}}|\mathrm{EX})}, \quad (17)$$

where $P(\hat{A}|B)$ is the probability an event is identified as source type A given the true source type is B; $\widehat{\mathrm{NoID}}$ indicates that an identification was not possible.

The study consisted of 5000 iterations. For each, a random sample of 80% of the events was selected from the NTS data. These data represent historic or calibration events and provided the measurements to calculate the necessary multistation discriminant parameters (τ and σ for P_g and L_g, along with ρ) for both populations, as well as decision rules (lines) for the three discrimination approaches. For each approach, the variability was assumed equal for both source types, giving a linear discrimination decision rule for all three. In the calibration component of an iteration, data are used to compute discriminant parameters; with these parameters in hand, event discriminants are calculated and decision rules are developed. For the multistation discriminant, $Z_{\bar{P}_g - \bar{L}_g}$ values are calculated. For both of the single-station approaches, only the station discriminant $X = P_g - L_g$ is calculated (e.g., no station averaging). The decision rule (line) for the multistation discriminant is simply the mean of the two source-type means, that is, $(\bar{Z}_{\mathrm{EX}} + \bar{Z}_{\mathrm{EQ}})/2$. For the single-station approaches, the decision rule (line) for each station is calculated as $(\bar{X}_{\mathrm{EX}} + \bar{X}_{\mathrm{EQ}})/2$; with this decision rule, an FDR can be calculated for each station. The best single station is then the one with the lowest FDR. Ties were broken by choosing the station with the highest $P(\widehat{\mathrm{EX}}|\mathrm{EX})$.

The remaining 20% of events in each iteration served as test data and can be viewed as new events requiring identification analysis. The discriminant parameters calculated from the 80% calibration data were used to compute the discriminants for the test data events; then, the decision rules

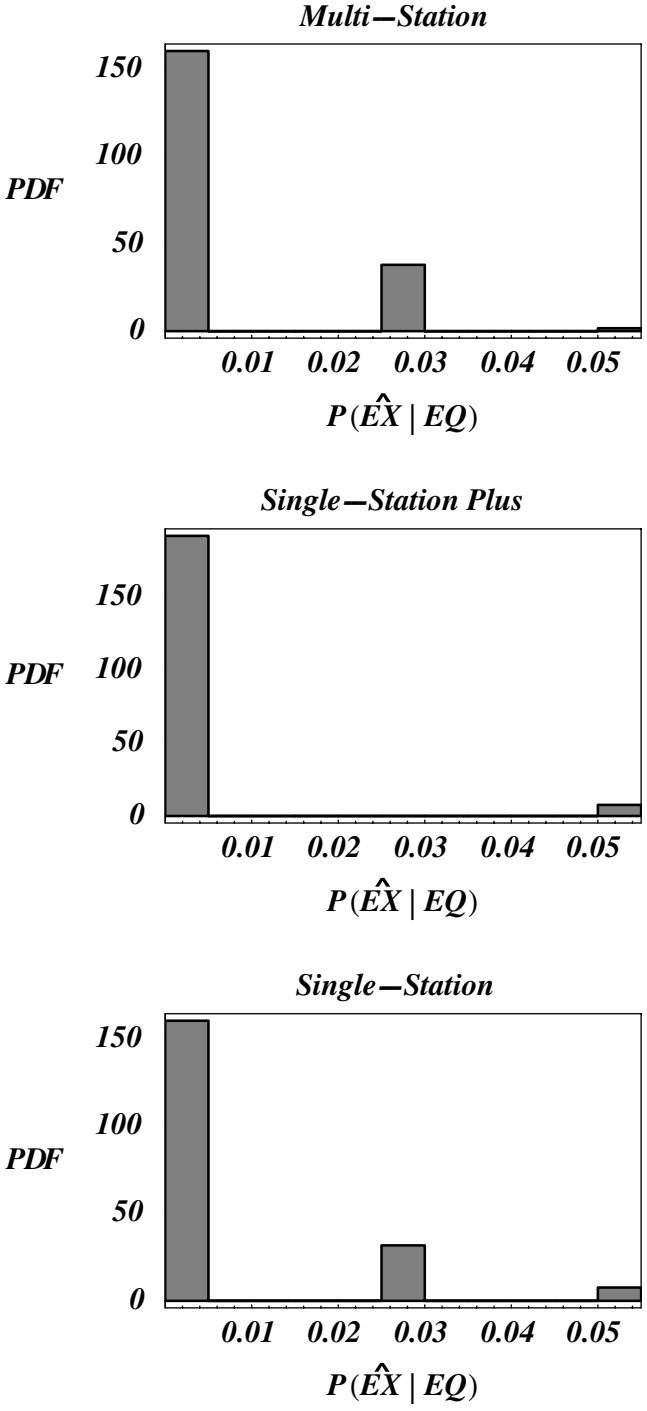

Figure 15. Operational burden for the multistation discriminant, along with the single-station and single-station plus approaches to regional discrimination. Histograms are from 5000 cross-validated values of the $P(\widehat{\mathrm{EX}}|\mathrm{EQ})$ component of operational burden.

developed from the calibration events were applied. If a test event is not observed by the best single station, an identification is not possible. In the single-station plus approach, if an event is not observed by the best single station, the decisions from the remaining stations are used—a simple vote with the majority providing the event identification. If only one of the remaining stations sees the new event, its decision is used as the event identification. If the remaining stations are in conflict (no majority), then no identification (NoID) is logged. For all three approaches, the predicted source type was then compared to the true type.

FDR results are summarized in Figure 12. One can see the multistation discriminant far outperforms the single-station approach and also represents an improvement over the single-station plus approach. The results of a closer look with FDR for only the multistation and single-station plus approaches are presented in Figure 13. The two FDR components are operational burdens in the numerator; the probability of correctly identifying an explosion is in the denominator. FDR is reduced as operational burden decreases. The part of operational burden resulting from no identification is summarized in Figure 14. The results emphasize a serious limitation of the single-station approaches—an unacceptably high no-identification rate. Because data from all stations are used in the multistation discriminant, source type can be predicted for all events. The other part of the operational burden comes from the probability of calling an earthquake an explosion. These results are summarized in Figure 15 and suggest that the performance of the single-station approach is slightly better than the other two approaches.

FDR is reduced as the $P(\widehat{\mathrm{EX}}|\mathrm{EX})$ increases. These results are summarized in Figure 16. Here, the multistation discriminant has significantly better performance than the single-station approach and also represents an improvement over the single-station plus approach.

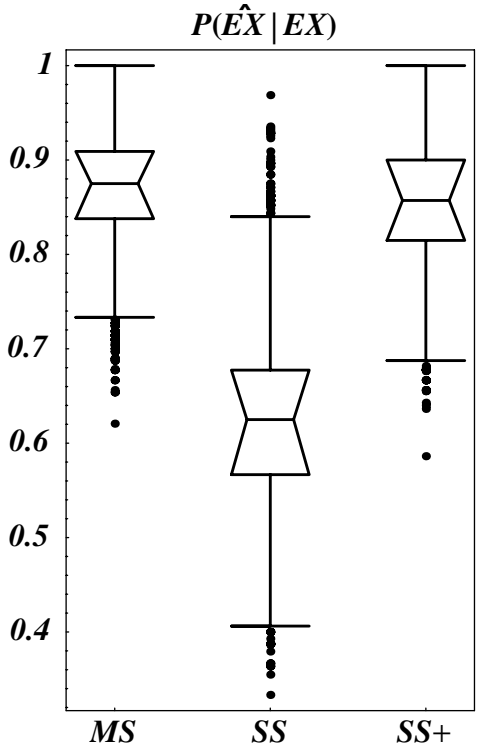

Figure 16. Box plots of 5000 cross-validated values of $P(\widehat{\mathrm{EX}}|\mathrm{EX})$ for the multistation (MS) discriminant, along with the single-station (SS) and single-station plus (SS+) approaches to regional discrimination.

Summary

We have developed and demonstrated a new approach to the regional seismic discrimination problem for nuclear explosion monitoring. In many ways, the method is analogous to that of the m_b versus M_s discriminant that has been in use for many decades. The idea is to individually correct observed station phase amplitudes (as a function of frequency) for path and earthquake source scaling using MDAC. Resulting amplitude corrections are then averaged over all observing stations prior to forming a ratio. This approach contrasts sharply with that of computing a phase ratio discriminant at individual stations. In the latter case, only stations that observe both phases or amplitudes are used, thereby excluding many potential measurements at additional stations. Research to develop regional amplitude-based discriminants for nuclear explosion monitoring has focused on theory development for seismic amplitude corrections. This article develops a general model for corrected amplitudes that properly includes correction model inadequacy and station noise as sources of error. This random effects model correctly gives the standard error of a multistation discriminant with a lower bound that conforms to physical basis, that is, the standard error will not become unrealistically small with an increase in observing stations. No source and path correction method is perfect, and model inadequacy is always present in a discriminant. Future developments include partitioning the error for the m_b versus M_s discriminant, which will result in a standard error analogous to equation (12).

Data and Resources

The data used to illustrate the discriminant $Z_{\bar{P}_g-\bar{L}_g}$ (equation 13) are events at and surrounding the Nevada test site (NTS). Events were observed with combinations of four seismic stations: Kanab, Utah (KNB), Elko, Nevada (ELK), Landers, California (LAC), and Columbia College, California (CMB). MDAC amplitudes from these stations were averaged in the calculation of $Z_{\bar{P}_g-\bar{L}_g}$. P_g and L_g amplitudes were pseudospectral measurements with a 6–8 Hz filter window. After applying data quality metrics (e.g., signal to noise and removal of events within 100 km of a station), the data table consisted of 41 earthquakes (EQ) and 159 explosions (EX) for a total of 200 events. Moment magnitudes (M_w) ranged from 2.6 to 6.1 for earthquakes and 2.8 to 5.9 for explosions. The spatial distribution of the events and stations is presented

in Figure 1. The data used in this article are openly available from the authors.

Acknowledgments

The authors acknowledge the support of Leslie A. Casey and the National Nuclear Security Administration Office of Nonproliferation Research and Development for funding this work. This work was completed under the auspices of the U.S. Department of Energy by Pacific Northwest National Laboratory under Contract Number DE-AC05-76RL01830. The authors also acknowledge the technical advice and historical perspective of Robert Blandford and Robert Shumway.

References

Blandford, R. (1982). Seismic event discrimination, *Bull. Seismol. Soc. Am.* **72,** 69–87.

Bonner, J., D. Russell, D. Harkrider, D. Reiter, and R. Herrmann (2006). Development of a time-domain, variable-period surface-wave magnitude measurement procedure for application at regional and teleseismic distances, part II: application and $M_s - m_b$ performance, *Bull. Seismol. Soc. Am.* **96,** 678–696.

Bottone, S., M. Fisk, and G. McCartor (2002). Regional seismic-event characterization using a Bayesian formulation of simple kriging, *Bull. Seismol. Soc. Am.* **92,** 2277–2296.

Brune, J. (1970). Tectonic stress and the spectra from seismic shear waves earthquakes, *J. Geophys. Res.* **75,** 4997–5009.

Chen, Y., and P. Tsai (2002). A new method of estimation of the attenuation relationship with variance components, *Bull. Seismol. Soc. Am.* **92,** 1984–1991.

Hartse, H., S. Taylor, W. Phillips, and G. Randall (1997). Regional event discrimination in central Asia with emphasis on western China, *Bull. Seismol. Soc. Am.* **87,** 551–568.

Lilliefors, H. (1967). On the Kolmogorov–Smirnov test for normality with mean and variance unknown, *J. Am. Stat. Assoc.* **62,** 399–402.

McLachlan, G. (1992). *Discriminant Analysis and Statistical Pattern Recognition*, Wiley and Sons, New York.

Searle, S. (1971). *Linear Models*, Wiley and Sons, New York.

Searle, S., G. Casella, and C. McCulloch (1992). *Variance Components*, Wiley and Sons, New York.

Stevens, J., and S. Day (1985). The physical basis of the m_b:M_s and variable frequency magnitude methods for earthquake/explosion discrimination, *J. Geophys. Res.* **90,** 3009–3020.

Taylor, S. (1996). Analysis of high-frequency P_g/L_g ratios from NTZ explosions and western U.S. earthquakes, *Bull. Seismol. Soc. Am.* **86,** 1042–1053.

Taylor, S., and H. Hartse (1998). A procedure for estimation of source and propagation amplitude corrections for regional seismic discriminants, *J. Geophys. Res.* **103,** 2781–2789.

Taylor, S., A. Velasco, H. Hartse, W. Phillips, W. Walter, and A. Rodgers (2002). Amplitude corrections for regional seismic discriminants, *Pure. Appl. Geophys.* **159,** 623–650.

Tsai, P., and Y. Chen (2003). Reduction of ground motion variability using the variance components technique, *EOS Trans. AGU* **84,** 46.

Tsai, P., Y. Chen, and L. Chia-Hsin (2006). The path effect in ground-motion variability: an application of the variance-components technique, *Bull. Seismol. Soc. Am.* **96,** 1170–1176.

Walter, W., and S. Taylor (2002). A revised magnitude and distance amplitude correction (MDAC2) procedure for regional seismic discriminants: theory and testing at NTS, Los Alamos National Laboratory Technical Report No. LAUR-02-1008.

Walter, W., K. Mayeda, and H. Patton (1995). Phase and spectral ratio discrimination between NTS earthquakes and explosions. part 1: empirical observations, *Bull. Seismol. Soc. Am.* **85,** 1050–1067.

Pacific Northwest National Laboratory
P.O. Box 999, MS K8-07
Richland, Washington 99352
dand@lanl.gov
(D.N.A.)

Lawrence Livermore National Laboratory
7000 East Ave.
Livermore, California 94550
(W.R.W.)

Pacific Northwest National Laboratory
902 Battelle Blvd.
Richland, Washington 99352
(D.K.F., T.M.M.)

Rocky Mountain Geophysics, LLC
128 Piedra Loop
White Rock, New Mexico 87544
(S.R.T.)

Manuscript received 2 April 2008